Title Page :

Measurement-based validation of a commercial Monte Carlo dose calculation algorithm for electron beams.

Previously

Clinical validation of the RayStation Monte Carlo dose calculation for electron beams using plane parallel radiation detectors.

Short Running title :

Electron Monte Carlo Code Clinical Validation

Geert Pittomvils (1), Evelien Bogaert (1), Erik Traneus (2), Pieternel Thysebaert (3), Carlos De Wagter (1)

(1) Ghent University Hospital, Corneel Heymanslaan 10, 9000 Gent, Belgium
(2) RaySearch Laboratories AB, Eugeniavägen 8, 113 68 Stockholm, Sweden
(3) Odisee Hogeschool-Universiteit Brussel, Bleekerijstraat 23-29, 1000 Brussel, Belgium

Author to whom correspondence should be addressed.

Geert Pittomvils, Corneel Heymanslaan 10, 9000 Gent, Belgium;
Electronic mail: geert.pittomvils@uzgent.be

Measurement-based validation of a commercial Monte Carlo dose calculation algorithm for electron beams

Geert Pittomvils (1), Evelien Bogaert (1), Erik Traneus (2), Pieternel Thysebaert (3), Carlos De Wagter (1)

(1) Ghent University Hospital, Corneel Heymanslaan 10, 9000 Gent, Belgium
(2) RaySearch Laboratories AB, Eugeniavägen 8, 113 68 Stockholm, Sweden
(3) Odisee Hogeschool-Universiteit Brussel, Bleekerijstraat 23-29, 1000 Brussel, Belgium

Abstract

Purpose : This work presents the clinical validation of RayStation's electron Monte Carlo Code by use of diodes and plane parallel radiation detectors in homogenous and heterogeneous tissues. Results are evaluated against international accepted criteria.

Methods : The Monte Carlo based electron beam dose calculation code was validated using diodes, air filled and liquid filled parallel radiation detectors on a Elekta Linac with beam energies of 4,6,8,10 and 12 MeV. Treatment setups with varying SSD's, different applicators, various cut-outs and oblique beam incidences were addressed, together with dose prediction behind lung, air and bone equivalent inserts. According to NCS (Netherlands Commission of Radiation Dosimetry) report 15 for non-standard treatment setups a dose agreement of 3 % in the δ_1 region (high dose region around Z_{ref}), a distance to agreement of 3 mm or a dose agreement of 10 % in the δ_2 region (regions with high dose gradients) and 4 % in the δ_4 region (photon tail/low dose region) were applied. During validation, clinical routine settings of 2x2x2 mm^3 dose voxels and a statistically dose uncertainty of 0.6% (250 000 histories/cm^2) were used.

Results : RayStation's electron Monte Carlo code dose prediction was able to achieve the tolerances of NCS report 15. Output predictions as function of the SDD improve with energy and applicator size. Cut-out data revealed no field size neither energy dependence on the accuracy of the dose prediction. Excellent agreement for the oblique incidence data was achieved and maximum one voxel difference was obtained for the distance to agreement behind heterogeneous inserts.

Conclusions : The accuracy of RayStation's Monte Carlo based electron beam dose prediction for Elekta accelerators is confirmed for clinical treatment planning that is not only performed within an acceptable timeframe in terms of number of histories but also addresses for homogenous and heterogeneous media.

Key Words : external beam electrons, Monte Carlo dosimetry, dose measurement, multi-dimensional chamber arrays, Phantoms for dosimetric measurement

1 Introduction

Radiotherapy by means of electrons remains essential, especially for superficial lesions, regardless the introduction of specialized photon techniques such as VMAT and IMRT or protons. The distinct longitudinal dose fall off in the electron depth behavior spares deeper lying tissues[1,2,3,4].

The dose calculation remains difficult to predict using analytical planning algorithms for non-standard setups. Non-standard setups include extended Source to Skin Distances (SSD), oblique incidences and heterogeneous tissues[3,5,6]. Monte Carlo based electron dose calculation methods have been introduced in commercial treatment planning systems during the last decade to resolve the challenge of accurate dose prediction for such non-standard setups[3,7,8]. More recently a study was published validating the Monte Carlo code of RayStation for a Varian accelerator relying on EBT film dosimetry in heterogeneous phantoms[9].

The RayStation (RaySearch Laboratories AB, Stockholm, Sweden) treatment planning system (TPS) was introduced at Ghent University Hospital in 2016 for an Elekta Synergy linac. The TPS is used for both Collapse Cone Photon dose prediction and Monte Carlo Electron dose prediction. For electron dose prediction the system uses a Monte Carlo-based beam model and the VMC++ code for in patient transport simulation[10]. To evaluate the accuracy of electron dose prediction by the commissioned system, the international guidelines for Quality Assurance of Treatment Planning Systems (TPS) of the Dutch Committee on Radiation Dosimetry (NCS, report 15) were followed[11].

2 Material and Methods

2.1 The RayStation Electron Monte Carlo Code

The electron dose calculation consists of two independent modules: a beam transport Monte Carlo model and the VMC++ Monte Carlo code for in patient transport simulation and dose reporting. Direct electrons are sampled from parameterized effective energy and spatial-angular distributions

accounting for the elements of a dual scattering foil beam line. The electron transport starts at the plane of the secondary scattering foil. At this plane, “direct” electrons are sampled (energy, position and direction) from a phase space defined by an analytical probability function. We treat energy and spatial-angular variables as independent i.e. the same energy spectrum is applied over the plane of the secondary scattering foil. The energy spectrum is defined by an analytical function with six parameters with values determined by an optimization procedure where a computed electron IDD is fitted to an open field (no applicator, jaws/MLC maximally retracted) electron depth dose. For the spatial part, the position and direction of an electron is sampled from a parametrized probability density function with five parameters. The surface of the secondary scattering foil is covered by an electron fluence density specified by a rotational symmetric Gaussian with a certain radial sigma and a cut-off-radius. At the cut-off-radius the fluence drops to zero. A virtual source point located on the beam axis upstream of the secondary scattering foil define an average direction of electrons created on point of the secondary scattering foil. Hence, on average all electrons point back the common virtual source point. Finally, the direction of an electrons is smeared out according to a radial Gaussian emittance distribution with a sigma varying as a decreasing linear function of the distance to the beam axis. In conclusion, the spatial-angular phace space is thus specified by in total five parameters; fluence, radial sigma, cut-off-radius, virtual source point, emittance linear function. All parameters are determined at beam modeling and are unique per linac and nominal energy. Direct electrons are further transported through a linac treatment head represented by a sequence of geometry objects with multiple scattering in air modelled according to the Goudsmit-Saunderson theory[12,13]. Direct electrons that impacts a collimating element (jaws/MLC/applicator/cut-out) are killed. A subset of the collimating elements may yield out-scattered “indirect” electrons which are transported like the direct electrons towards the exit of the treatment head. Elements that can produce indirect electrons are the applicator scraper layers and the cutout. The out-scatter electrons are generated by a dedicated Monte Carlo code developed specifically for this purpose. The photon contamination dose, mainly arising from bremsstrahlung in the scattering foils, is computed by a fast

semi-analytical 3D dose calculation algorithm using a Singular Value Decomposition method (SVD). The SVD dose engine is based on the pencil beam convolution technique and can be considered equivalent in terms of accuracy. A pencil beam kernel is approximated by three components that are separable in depth and lateral directions. This separation eliminates the need for three-dimensional convolutions which increases calculation speed, as was first described for the purpose of dose calculation by Bortfeld et al.[14]. A photon contamination depth dose input to the IDD is computed according to the approximate method described in literature[15]. The photon contamination lateral fluence is modelled as a rotational symmetric Gaussian distribution with attenuation to account for the cut-out aperture and the geometry of the most downstream scraper. The VMC++ code is optimized for three-dimensional dose calculations in voxel geometries and uses a class II condensed history (SH) scheme for the simulation of charged particle transport. Hence, bremsstrahlung interactions that result in the creation of photons above threshold, and inelastic scattering that sets in motion secondary electrons with energy above threshold, is treated discretely by creation and transport. Sub-threshold inelastic processes are accounted for using the Continuous Slowing Down Approximation (CSDA). In VMC++ transport parameters are determined at runtime and adapts to voxel size and beam quality. Relevant parameters for MeV electron beams are the delta electron threshold (typical value 250 keV), photon transport threshold (typical value 50 keV).

The VMC++ code is setup to score dose to water obtained by a stopping-power-ratio (SPR) correction factor applied during transport at every energy accumulation. The SPR factor is computed in the actual medium per voxel at a representative energy the electron has while crossing the voxel. The SPR is computed at the average energy (computed as average of energy when entering and exciting the voxel). For further details the reader is referred to reference books and the references therein[10].

2.2 Preliminary beam modelling process and reproducibility study

The Elekta Synergy platform (Elekta, Crawley, UK) has available electron treatment energies of 4, 6, 8, 10, 12 MeV for a set of square applicators measuring 6x6, 10x10, 14x14, 20x20 cm^2. This linac in electron mode is exclusive in its configuration, because it uses a unique jaw setting per applicator and energy, in combination with a very light applicator design. This applicator consists out of multiple scrapers levels that gradually reduce the field size defining it at an SSD of 95 cm[16].

Measurements in water and air are necessary for creation of the electron beam model in the Rayphysics module of RayStation version 6.0. The different measurement setups that have been used are:

- Roos plane parallel chamber (type 34001-PTW Freiburg) for Percent Depth Dose curves (PDDs) in water, converted from the ionization data using the DIN6800-2 protocol in the PTW Mephysto software[17].
- Semiflex cylindrical chamber (type 30010; PTW Freiburg) with buildup cap for relative cross- and in-plane fluence ionization profiles in air at two SDD distances (70-90cm).
- Diamond detector (type 60003; PTW Freiburg) for cross- and in-plane relative ionization profiles in water.

As already described in literature the machine definition in RayStation is very detailed covering a large set of different parameters in the machine head, and all applicator and jaw setting differences for each energy and applicator[9].

In the modelling performed in the Rayphysics module of RayStation 6.0, the photon dose tail contribution is expressed as a percentage of the total dose using integer values resulting in a relative inaccuracy of the photon tail modelling of up to 30 % for the lowest energies. The beam modelling using the VMC++ dose engine of the Elekta Linac resulted in an absolute dose inaccuracy around d_{max} of 1% for most energies, 2% differences were observed for 4 MeV. The Distance To Agreement (DTA) in the dose fall off region of the PDD was 1mm or smaller for all energies and applicators. The

observations during the modelling of the Elekta Linac were similar to the ones reported for the Varian True Beam[18], where field widths and penumbra shapes are good matches as is the dose profile within the 80% of the Beam Profile. The modeling of the Elekta linac resulted in an excellent match of the out-of-field dose. Also the shoulder regions are predicted accurately, beside for 4 MeV and 6 MeV where a slight overestimation by the TPS is apparent, a trend that is reported for all beam energies of the Varian Linac[18]. Once this modelling in the Rayphysics module is performed the validation can start in the RayStation planning module.

All calculations were performed in a calculation grid size of 2x2x2mm³ and collimator setting was 0° for all setups.

Before validating the model in the RayStation planning module, an evaluation of the statistical accuracy of the Monte Carlo dose engine was performed. The reproducibility of dose ameliorates with increasing number of histories (dose uncertainty decreases roughly by inverse square root of number of histories). A field size dependent number of 250 000 histories per cm^2 can be run within an acceptable calculation time of less than 15 minutes and yields a dose uncertainty standard deviation of 0.6% (reported as the average standard error for all voxels with more than 50% of the max. dose per field). For example, using 1 000 000 histories per cm^2 results in a dose uncertainty of the order of 0.3%, but would increase overall validation time by a factor of four. Therefore 250 000 histories per cm^2 was selected for this study.

Following the NCS18 guidelines, which are based on water to air stopping power ratio's, absolute dose calibration (1 cGy=1 MU) was performed at Reference Depth (Z_{ref}) for each beam quality at a Source to Surface Distance (SSD) of 95 cm[19]. This distance is identical to the distance between the source and the distal end of the Elekta applicators, omitting an air gap in reference conditions.

NCS-15 acceptance criteria on treatment planning systems for electron beams are described not only in the report itself[17], are also summarized in a recent study validating RayStation's electron Monte Carlo algorithm for a Varian Truebeam accelerator[18]. Here the different regions are explained: the δ_1

region (high dose region around Z_{ref}), the δ_2 region (regions with high dose gradients) and the δ_4 region (photon tail/low dose region).

2.3 SSD dependence of dose output

According to Saw et al. the shape of the PDD curve from and beyond the point of maximum dose is not affected by the effects of extended SSD[4]. The main effect of an increased SSD is a reduction of dose output with increasing SSD. Thus, dose output prediction has been validated against measurements for SSD values ranging from 95.5 cm to 115 cm, admitted within RayStation. For this purpose, the reference plane chamber (Roos PTW, Freiburg) was used in a Z_{ref} setup in a polystyrene phantom (25x25x15cm³) for all four available applicators; 6x6, 10x10, 14x14, 20x20 cm².

2.4 Dose output for different cutouts

The dose output for 19 different cutouts was verified at a depth of Z_{ref} and at SSD = 100 cm, using a Diode E, type 60012 of PTW in a large water tank (MP3 PTW). The obtained field sizes range from 16 cm² (4x4 cm² on the 6x6 cm² applicator) to 400 cm² (20x20 cm² on the 20x20 cm² applicator). A cross-calibration for the doses obtained by both the Diode E and the Roos chamber was performed for the standard cutout for every applicator at Z_{ref} depth and SSD = 100 cm. This cross calibration eliminated small setup errors, as the large water tank had to be repositioned after each applicator exchange, making the results more specific for the influence of the cutout on the dose output.

2.5 Oblique incidence

The main change in the depth dose profile with increasing obliqueness is the decrease of the R50 value[8]. This implies that the dose at the depth of the “standard R50” value will drop with increasing obliqueness. This dose drop was measured by the electron diode in vertical orientation with the phantom at SSD = 110 cm in order to avoid collision (see figure 1).

In order to keep the diode detector entirely exposed by the 14x14cm^2 incident beam upon increasing angle of incidence (from 0° to 30°), a fixed position of the phantom with a unique lateral

displacement of 4 cm more distal to the beam axis was applied (see figure 1). Directional response of the dosimetry diode, ranging from 0.98 to 1.00, was taken into account using the user manual data of the PTW electron diode.

Absolute dose was obtained by applying dose correction values for the electron diode in the phantom material in reference conditions.

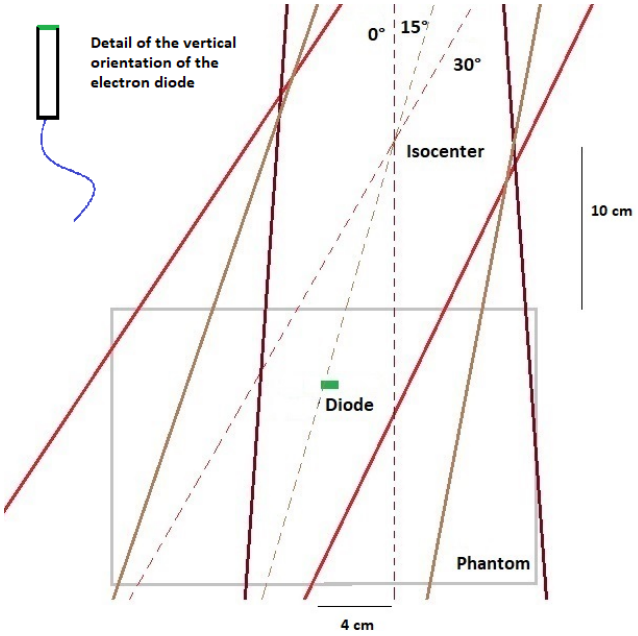

Figure 1 : Setup for oblique beam incidence measurements. A 4 cm offset was introduced in order to keep the diode exposed for each beam incidence.

2.6 Dose behind heterogeneous media

Validation of dose behind heterogeneous media is performed with lung, air or bone inserts surrounded by polystyrene and a linear detector array (type LA48, PTW, Freiburg)[20]. The linear detector array consists of 47 4x4x0,5 mm^3 liquid ion chambers positioned every 8 mm. It was embedded in a 35x25x10 cm^3 polystyrene slab holder placed horizontally underneath the heterogeneity inserts at different distances. During the validation process, both the slab holder and the linear array are considered an integral part of the phantom. Both generate phantom scatter dose and the linear array induces significant back scatter dose because it is constructed from high-density materials and are therefore included in the CT-image data set.

Dose data points measured by the linear detector array were compared with the non-interpolated line dose calculated by RayStation. Absolute dose was obtained by applying correction factors for the linear array in the phantom material in reference conditions.

2.6.a Lung

The lung phantom consists of eight 14x14 cm^2 polystyrene slabs with central lung inserts (LN300 Gammex) of sizes 6x6 cm^2 and 4x4 cm^2 with a mass density of 0.29±0.5 g/cm^3 (see figure 2). This results in 1 cm build up material proximal to the lung insert.

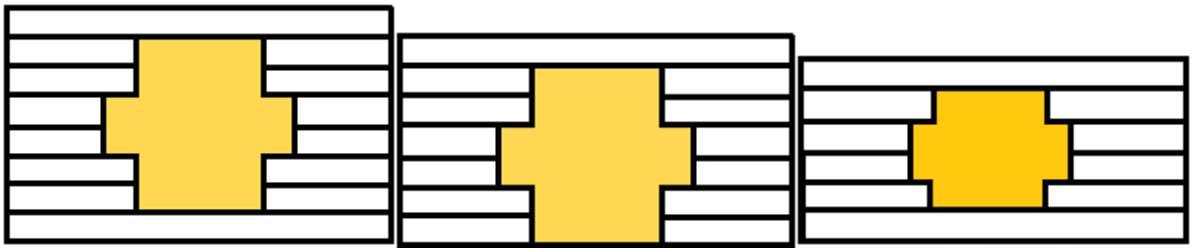

Figure 2. Left: Lung phantom with buildup on top of the linear detector array. Center: Lung phantom without build up on top of the linear detector array; Right: air phantom. Beam direction is top down. Slab thickness is 1 cm and sagittal and axial views are identical.

To evaluate the effect of the lung tissue on the dose distribution, the calculated dose behind the insert was compared with the measured dose using the PTW linear detector array. This was done at two depths: first with a 1 cm polystyrene buildup slab on top of the linear detector array and, secondly, without the buildup slab. Three applicator sizes (6x6 cm^2, 10x10 cm^2, and 14x14 cm^2) combined with the five available energies, resulted in thirty dose profiles to be analyzed. An SSD of 100 cm was maintained.

2.6.b Air

The air insert phantom consists of six polystyrene slabs of 14x14 cm^2 where the two central slabs have 5x5 cm^2 central openings and the adjacent slabs (one proximal, one distal) 3x3 cm^2 openings. This results in 1 cm buildup before and behind the air cavity (see Figure2). Three applicator sizes

combined with five energies resulted in fifteen dose profiles to be analyzed at a depth of 1 cm behind the air cavity.

2.6.c Bone

Three bone rods (length 7 cm, diameter 2.9 cm) belonging originally to the Tissue Characterization Phantom Model 467 (Gammex, Middleton, USA) and with different densities are mounted in a polystyrene slab based holder of 15x15x3.5 cm^3, resulting in three different bone phantom CT-scans.

These inserts have electron densities relative to that of water (ρ_{EDW}) of 1.28, 1.47, and 1.69 with corresponding mass densities of 1.332 g/cm^3, 1.559 g/cm^3, and 1.810 g/cm^3, respectively. Two different applicators of sizes 10x10 cm^2 and 14x14 cm^2 were used at five electron energies. This bone setup was again placed on top of the linear detector array in its holder. In total 30 dose profiles were analyzed.

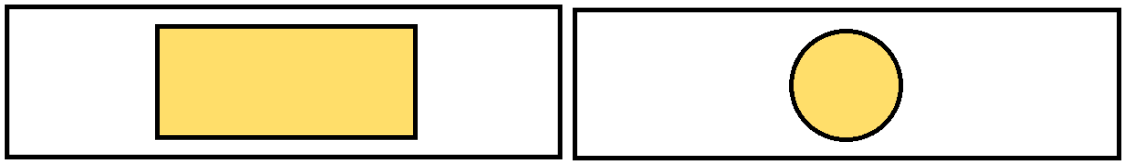

Figure 3 : GT (in-plane) and AB (cross-plane) cross sections of the bone phantom. Beam direction is top down.

3 Results

3.1 SSD dependence of dose output

A total number of 96 measured output factors (cGy/MU) was compared at Z_{ref} with values calculated by RayStation. Only 2 values out of 96 exceed the 3% tolerance level but remain below 3.5%. It concerns dose output values for low energies (4-6 MeV) for the smallest applicator. Eighteen measurements and 18 calculated values are depicted in Figure 4 illustrating the very good agreement (within 2%) between measured and calculated data for large applicators (≥10x10cm^2) and/or high energies (≥8 MeV) and the observed deviation for the smallest applicator at low energies.

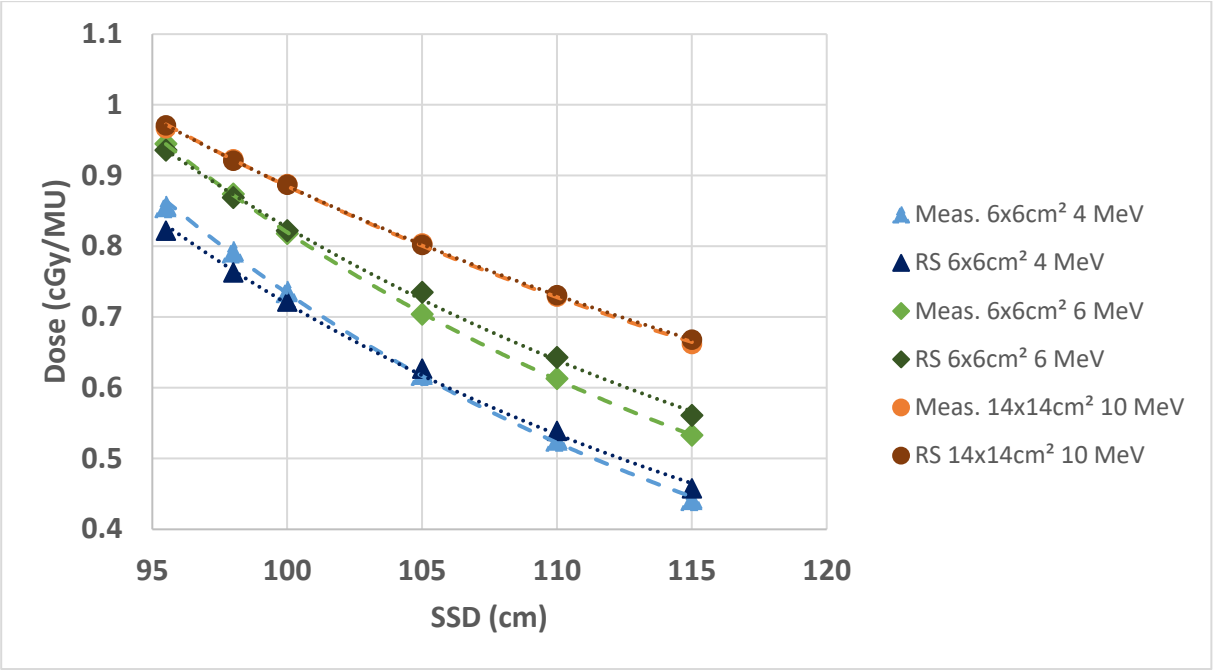

Figure 4 : SSD dependence of the dose output at Z_{ref}. Data measured with the Roos chamber (Meas.) are compared with calculated data (RS)

3.2 Dose output for different cutouts

All the 95 relative raw data points obtained with the diode at Z_{ref} are within the 3% tolerance of the NCS-15 report. However, systematic differences were identified linked to the repositioning of the phantom during the applicator exchange. Cross-calibration of the diode data with the reference data of the standard cut-outs measured with a Roos chamber, resulted in a reduction of the average difference between the measured and calculated data from 1.5%±1.0% to 0.5%±0.8%.

The agreement between calculation and measurement of the small cutouts of the smallest applicator are equivalent to the agreement for the larger cutouts proving the robustness of the planning algorithm. Even the dose prediction of cutouts with a width of only 2.5 cm (2.5x10cm² on a 10x10cm² applicator) have equivalent accuracy (0.04%±0.8%) as the standard cutout (0.5%±0.6%) despite the large change in beam efficiency (7-11 %). No dependence of energy or applicator type on the dose output accuracy is observed, the average agreement for all those parameters remains within 1.0% in dose difference.

Energy	4MeV		6MeV		8MeV		10Mev		12Mev	
	Meas.	RayStation	Meas.	RayStation	Meas.	RayStation	Meas.	RayStation	Meas.	RayStation
Applicator size (cm²) cutout size (cm²)	Dose (cGy/MU)	Dose (cGy/MU)	Dose (cGy/MU)	Dose (cGy/MU)	Dose (cGy/MU)	Dose (cGy/MU)	Dose (cGy/MU)	Dose (cGy/MU)	Dose (cGy/MU)	Dose (cGy/MU)
6 x 6										
6 x 6; 36 cm²	0.814	0.801	0.903	0.901	0.950	0.959	0.968	0.977	0.991	0.996
4 x 6; 24 cm²	0.815	0.809	0.901	0.909	0.951	0.944	0.951	0.947	0.982	0.978
4 x 4; 16 cm²	0.805	0.802	0.885	0.905	0.926	0.937	0.932	0.936	0.946	0.949
10 x 10										
10 x 10; 100 cm²	1	1	1	1	1	1	1	1	1	1
7 x 10; 70 cm²	0.999	0.995	0.996	1.000	0.999	1.008	0.998	1.006	0.997	1.006
8 x 8; 64 cm²	0.991	0.997	0.990	1.003	0.990	1.007	0.990	0.993	0.990	1.013
5 x 10; 50 cm²	0.990	1.000	0.987	0.993	0.987	0.994	0.983	0.985	0.982	0.985
4 x 10; 40 cm²	0.982	0.981	0.979	0.983	0.974	0.991	0.969	0.968	0.965	0.973
2.5 x 10; 25 cm²	0.933	0.933	0.922	0.933	0.916	0.914	0.902	0.890	0.889	0.893
14 x 14										
14 x 14; 196 cm²	1.046	1.057	0.991	0.994	0.987	0.995	0.977	0.979	0.979	0.987
12 x 12; 144 cm²	1.047	1.049	0.975	0.999	0.988	0.998	0.979	0.973	0.982	0.990
10 x 14; 140 cm²	1.053	1.051	0.981	1.001	1.008	0.999	0.984	0.980	0.986	0.993
8 x 14; 112 cm²	1.052	1.047	0.980	0.998	0.991	0.994	0.983	0.985	0.985	0.992
8 x 12; 96 cm²	1.056	1.041	0.991	1.005	0.996	1.007	0.987	0.967	0.990	0.996
4 x 12; 48 cm²	1.030	1.043	0.960	0.975	0.968	0.974	0.960	0.953	0.960	0.961
20 x 20										
20 x 20; 400 cm²	1.041	1.046	1.000	0.993	0.985	0.987	0.967	0.977	0.972	0.981
8 x 20; 160 cm²	1.038	1.049	0.997	0.992	0.984	0.994	0.970	0.977	0.977	0.980
6 x 20; 120 cm²	1.038	1.036	0.998	0.990	0.986	0.998	0.971	0.969	0.977	0.987
7 x 18.5; 129.5 cm²	1.039	1.041	1.001	1.001	0.986	0.990	0.972	0.973	0.978	0.988

Table 1 : Output factors for the different types of cutouts, calculated values versus measurements using an electron diode at Z_{ref}. All data are cross-calibrated using a Roos reference chamber for standard cut-outs.

3.3 Oblique Incidence

For each beam energy the calculated dose was compared to the measured dose at seven different incidence angles (0°-30° with steps of 5°) at a depth close to the respective "standard R50" value, that is a location in the high dose gradient part of the PDD curve (δ_2 region).

For 4 MeV the depth of calculation was set at 15 mm, for 6 MeV at 20 mm, for 8 MeV at 30 mm, for 10 MeV at 40 mm and for 12 MeV at 45 mm. One millimeter more proximal/distal were also measured for the low energies and one and two millimeter proximal/distal for 10 MeV and 12 MeV were also measured in order to find the best fit. Verification of the distance to agreement is more reliable than comparing dose differences in high dose gradient regions. The objective is to check

whether an distance to agreement of 2 mm or better can be obtained. For all energies and at all depths a decrease of dose with increasing angle of incidence is observed, as expected.

The best fit for the 4, 6, 8 and 12 MeV beam occurred at a depth identical to the depth of calculation (15, 20, 30 and 45mm). Although the best fit for the 10 MeV beam remained the depth of calculation (40mm), the distance to agreement was larger but remained below 1mm (see figure 5).

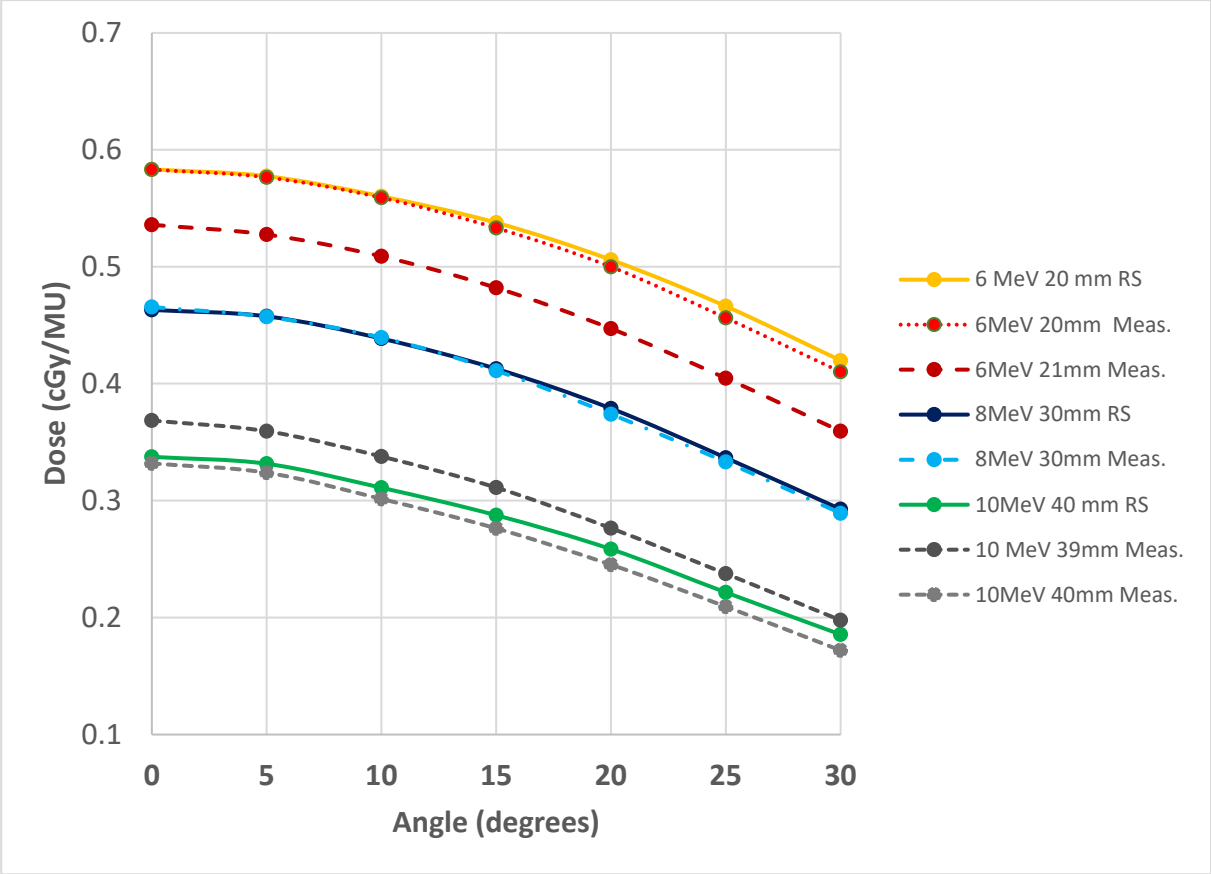

Figure 5: Dose ouput at SSD=110 cm with the electron diode around the "standard R50" depth values[17]. The solid lines are RayStation calculation values (RS), the dashed lines are doses measured at depths indicated in the legend. The depth values are in a high dose gradient region (δ_2 region) and there the distance to agreement is the standard criterium to evaluate the agreement between measured and calculated data. All data are within 2 mm tolerance (1mm or less).

3.4 Dose behind heterogeneous media

3.4.a Air

Figure 6 compares the measured dose 1.1 cm behind (1 cm due to the buildup layer plus 1 mm buildup inside the chamber before the air cavity) with the calculated line dose. Excellent agreement is obtained for al beam energies both in terms of distance to agreement (NCS15 δ_2 region; 3 mm) and in dose difference (NCS15 δ_2 region; 10%; δ_4 region; 4%). The best fit was obtained using the calculated data of the voxels exactly at the position of the ionization chambers.

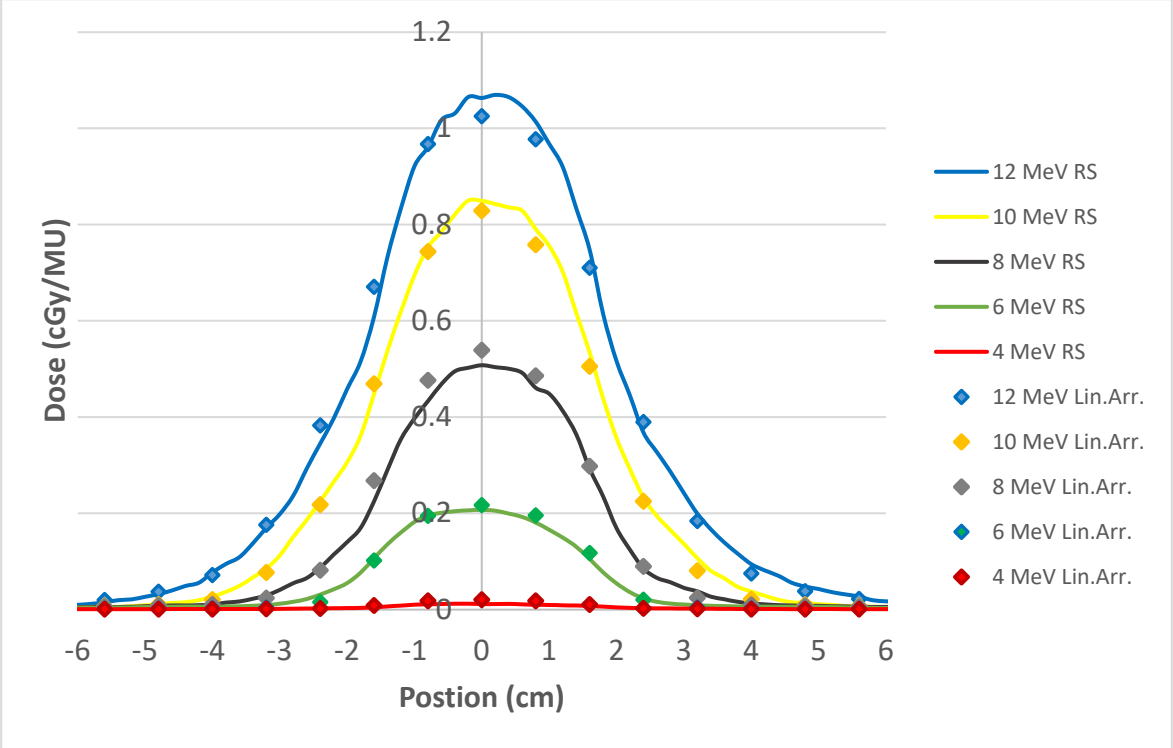

Figure 6: Dose profiles 1,1 cm behind the air cavity for beams at SSD=100 cm, calculated values (RS) versus measurements with the Linear Array (Lin.Arr.) for a 10x10cm² field for 5 different beam energies

The plus shape of the insert (cf. Figure 2) enables the validation of the beam modelling at different water equivalent depths (2.1 cm (at central axis); 4.1 cm (2 cm off axis); 6.1 cm (4 cm off axis)). Central axis data of the 10x10 cm² and 14x14 cm² beams of 12 MeV are exceeding 1 cGy/MU as illustrated by figure 6. PDD analysis of the calculated curves however confirm that at the level of the

linear detector array the dose decrease exceeds 3%/mm implying that at this position a δ_2 criterion has to be applied (NCS15).

3.4.b Lung

Line dose profiles behind the heterogeneous phantom are considered at two different depths below the lung-polystyrene interface (0.1 cm without buildup 1.1 cm with 1 cm buildup). Line dose profiles at the same depth as the liquid ion chambers do not always deliver the best agreement with the measurements. This line dose changes every 2 mm in depth due to the calculation grid of 2x2x2 mm³. Figures 7 and 8 show the line dose profiles for the best fit at the two depths (0 and 1 cm buildup) behind the lung-polystyrene interface. The use of identical depth for line dose extraction compared to the measurements usually generated the best fit but a shift of one calculation voxel in the line dose is sometimes necessary in order to obtain a good fit (cf. figure 7 and 8). All fits however remained within NCS 15 tolerances of 3 mm.

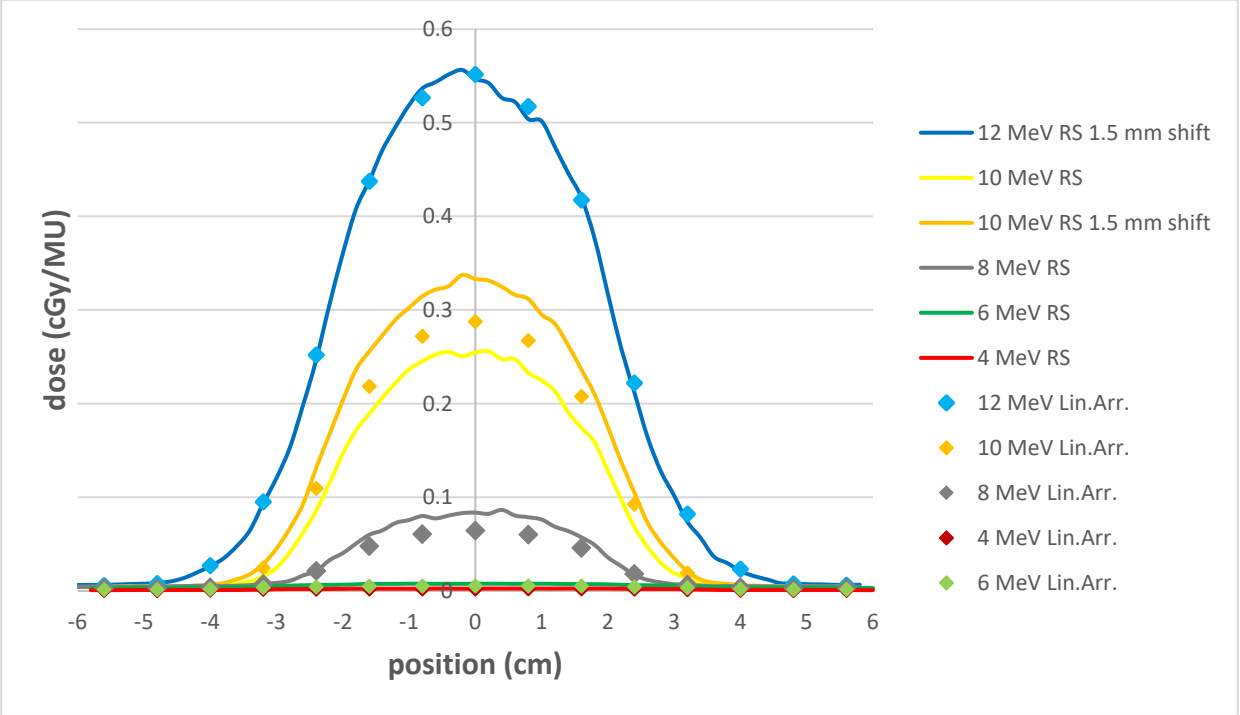

Figure 7 : Dose profiles 1,1cm behind the lung cavity for beams at SSD=100 cm, calculated values (RS) versus measurements with the Linear Array (Lin.Arr.) for a 6x6cm² field for 5 different beams energies. For 12 MeV best fit was obtained using a 1.5 mm shift more distal in the calculated curve and for 10 MeV both curves are as close to the measurements.

As for the air cavity, the plus shape of the lung insert (cf. figure 2) enables the validation of the beam modelling at different water equivalent depths. For the phantom without buildup along the central axis the water equivalent depth is 2.9 cm (1 cm polystyrene, 6 cm lung material, 1 mm chamber build up). For a displacement of 2.5 cm laterally along one of the primary axes the water equivalent depth becomes 5.7 cm (5 cm polystyrene and 2 cm lung material, 1mm chamber build up), and for a lateral displacement of 4 cm the water equivalent depth is 7.1 cm. For the phantom with a buildup layer of 1 cm between the lung cavity and the LA48 linear detector array those water equivalent values increase by 1cm to 3.9 cm, 6.7 cm and 8.1 cm.

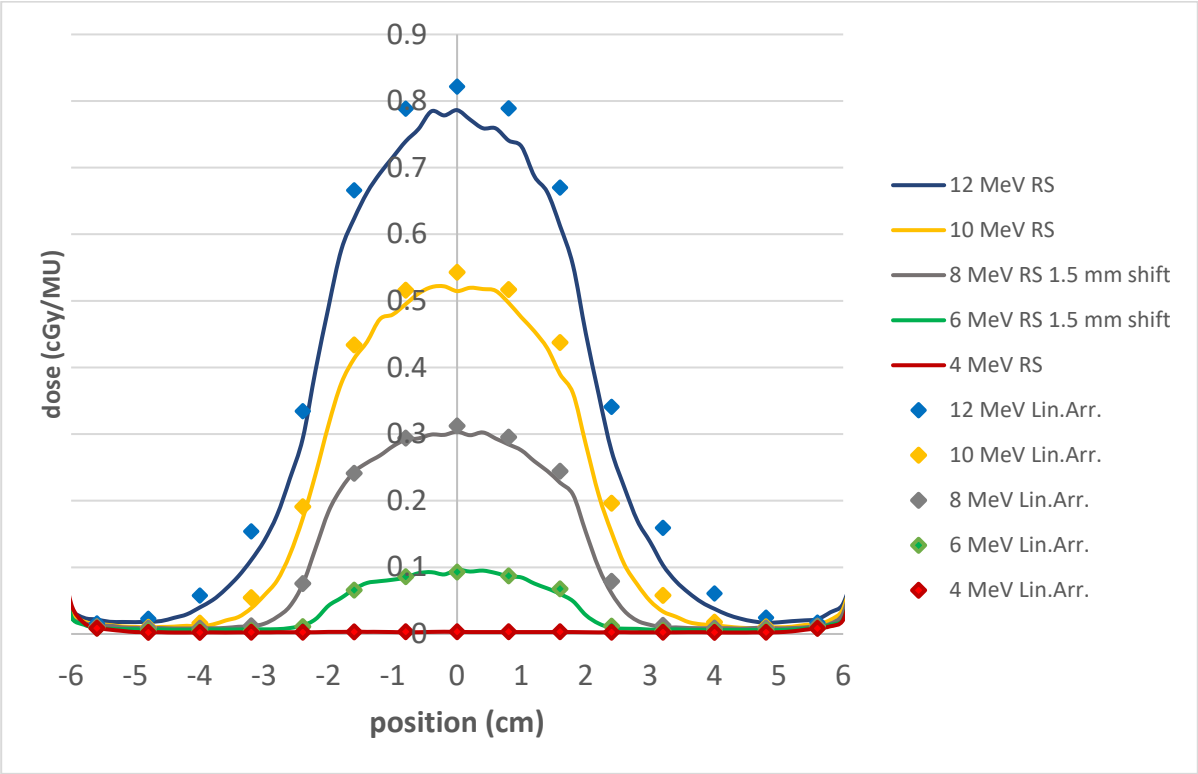

Figure 8 : Dose profile 1 mm behind the lung/polystyrene interface for beams at SSD=100 cm, calculated values (RS) versus measurements with the Linear Array (Lin.Arr.) for a 14x14cm² field for 5 different beams energies. For 6 MeV and 8 MeV best fit was obtained using a 1.5 mm shift more distal for the calculated curve.

3.4.c Bone

Tolerances for dose behind heterogeneous media are stated in NCS15 for δ_2 dose region as 10 % dose agreement/3 mm DTA and for the δ_4 region (photon tail) as 4% dose agreement without any specified DTA criteria. Dose behind the three bone inserts with different relative electron densities were evaluated against these criteria. For both applicators for the five different beam energies the agreements between calculated and measured data were within the tolerances of NCS15. Three different setups are depicted in Figures 9-11. Measured data are compared with non-interpolated calculated line profile values.

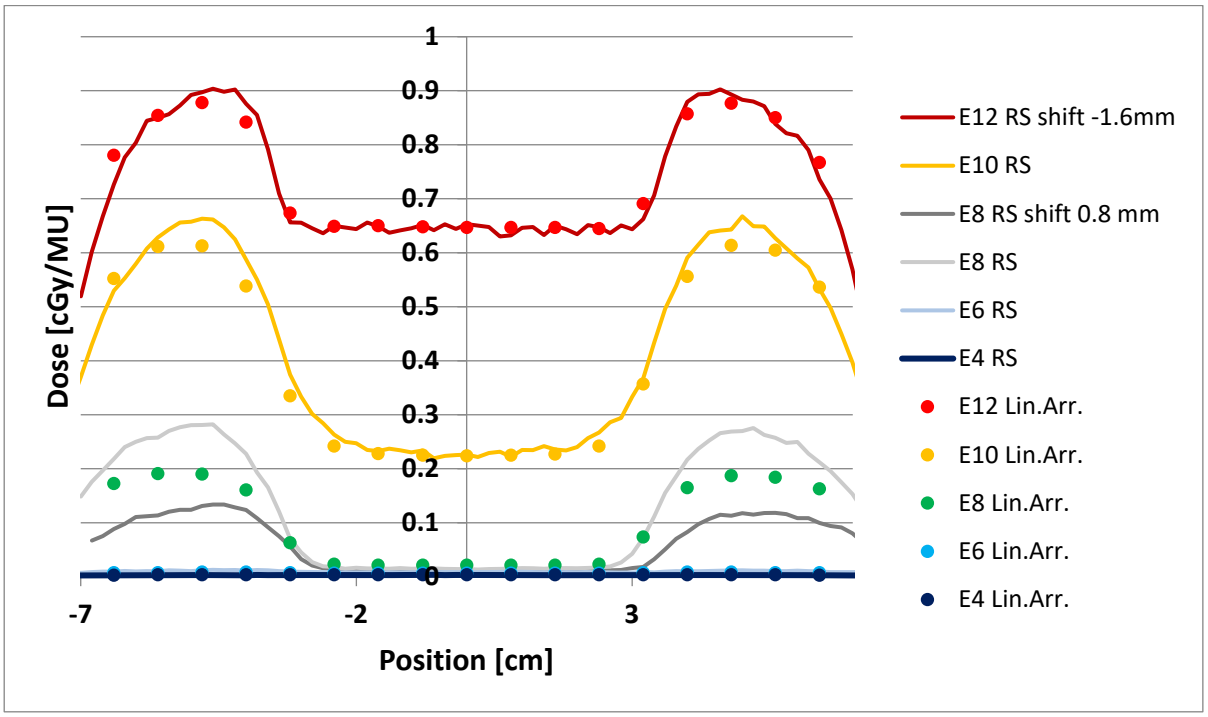

Figure 9 : Comparison of dose profiles, measured (Lin.Arr.) and calculated (RS) behind the phantom with a bone rod of ρ_{EDW} =1.28 for 5 electron beam energies (E4,E6,E8,E10,E12). Profiles are along the length axis of the rod for a 14x14cm² field

Figure 9 shows the dose profiles for the 14x14 cm² applicator along the length axis (GT direction (cf. Figure 3)) of the bone rod with a relative electron density of 1.28. For 4, 6 and 10 MeV the best fit between line doses and measurements was obtained at exactly the same depth. For 12 MeV the best fit was obtained for a line dose profile through one voxel-row more proximal, while for 8 MeV the

best fit was obtained for a line dose profile through one voxel-row more distal. The RayStation dose predictions were within NCS15 tolerances for positions both right behind the bone inserts and laterally to the insert. Please note that for 4 and 6 MeV only the photon tail agreement could be verified due to the dimensions of the bone phantom (thickness 35mm).

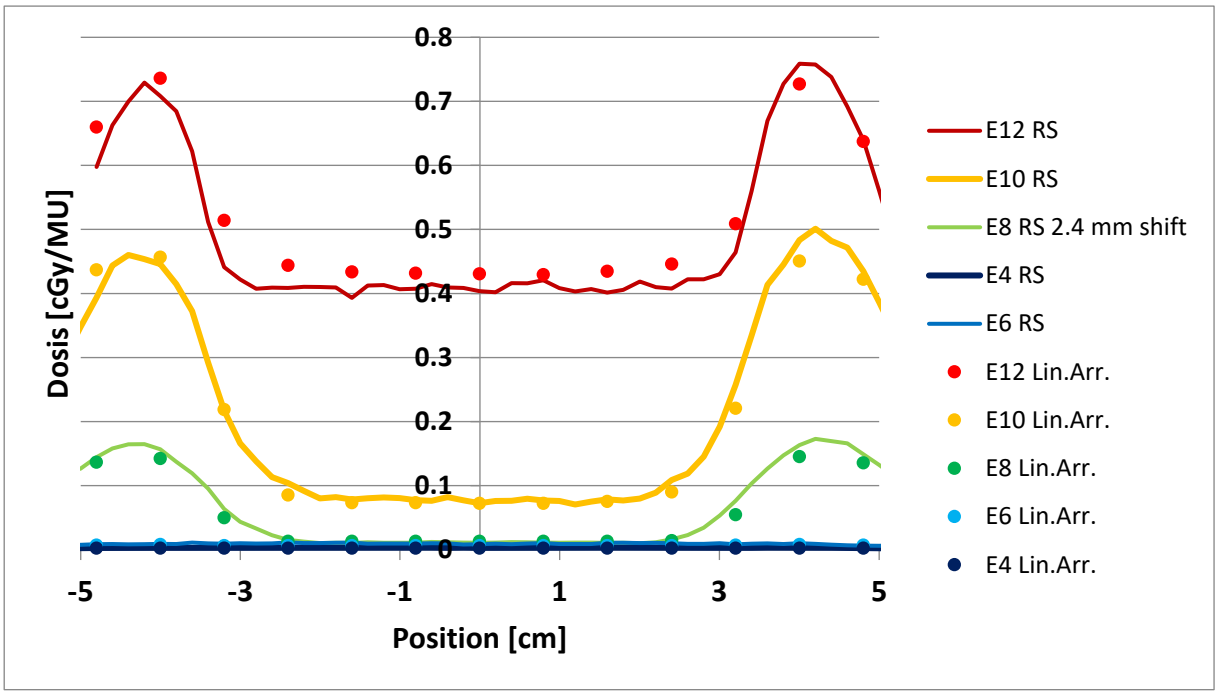

Figure 10: Comparison of dose profiles, measured (Lin.Arr.) and calculated (RS) behind the phantom with a bone rod of ρ_{EDW} =1.47 for 5 electron beam energies (E4,E6,E8,E10,E12). Profiles are along the length axis of the rod for a 10x10cm² field.

For the second and denser bone rod (ρ_{EDW} = 1.47), predicted dose and measured dose along the GT axis were investigated (see Figure 10). This higher density decreases dose behind the rod and the smaller field size (10x10 cm²) influences the shape and dose level lateral to the rod. Both effects are modelled by RayStation within the tolerances of NCS15. Best fit was obtained for the line doses calculated at measurement depth except for 8 MeV, there a shift of one calculation voxel was needed in order to obtain a good agreement.

The comparison of measured and calculated dose AB profiles (cf. figure 3) for the most dense rod (ρ_{EDW} = 1.69) are presented in Figure 11. Also in this case, the best fit was achieved for a line profile composed by the calculation voxels at the same depth or a depth at one voxel more proximal. The

dose absorption in this high density region is modeled correctly and the observed results are within the tolerances of NCS15 (10% dose agreement/3 mm DTA) for the δ_2 dose region and a dose agreement of 4% for the δ_4 region (photon tail). Note that the dose levels lateral to the rod are equivalent to the dose levels in Figure 9, as expected using in both cases 14x14cm² fields. Below the rod all but 12 MeV beams are evaluated in the photon tail region.

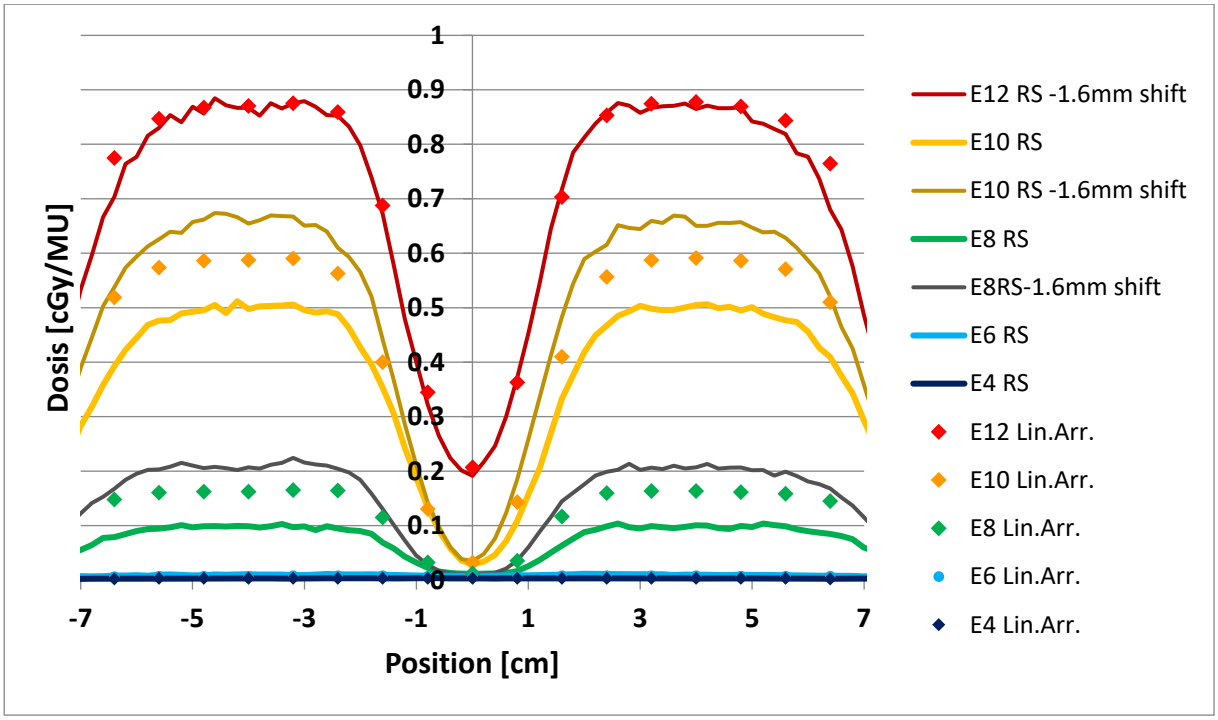

Figure 11: Comparison of dose profiles, measured (Lin.Arr.) and calculated (RS) behind the phantom with a bone rod of ρ_{EDW} = 1.69 for 5 electron beam energies (E4,E6,E8,E10,E12). Profiles are perpendicular to the length axis of the rod for a 14x14cm² field.

4 Discussion

4.1 SSD dependence of dose output

Data are available in literature modelling the SSD dependence following the inverse square law with an effective source position using the method of Khan[21] applied on data with a 10 cm larger SSD range of a different type of accelerator[22]. Similar to these data, for all applicators both RayStation

and measured data could be fitted with determination coefficients 0.995 or higher. The resulting effective source position values are listed in Table 2.

The accuracy of those values are however influenced by the small range in SSD (limited by maximal air gap in RayStation), resulting in an estimated uncertainty of around 1-2% on the fitted value. For a given energy, the effective SSD depends strongly on the collimator opening. For larger collimation openings the effective source position appears to deviate less form the nominal value of 95 cm. For a given collimation opening, the effective SSD depends on the energy of the beam. For small collimator openings (<14x14 cm^2), the lower the beam energy, the shorter the value of the effective SSD, for large applicator openings (≥14x14 cm^2) the SSD_{eff} is almost independent of energy. All those observations are in agreement with previous reported data of different accelerator types[22,23].

	6x6cm^2		10x10cm^2		14x14cm^2		20x20cm^2	
	Linac	RS	Linac	RS	Linac	RS	Linac	RS
4 MeV	50	57	74	77	84	86	90	89
6 MeV	59	68	80	85	87	88	92	91
8 MeV	65	71	86	90	90	93	93	94
10 MeV	71	73	88	87	94	94	96	95
12 MeV	71	80	86	92	94	94	96	94

Table 2: Estimation of the SSD_{eff} in cm of the virtual source fitted on the calculated ('RS') and measured ('Linac') data

Electron beams are shaped by the scrapers in the electron applicators[24] and for the Elekta accelerator four different scraper levels are present gradually limiting electron field size which depend on each selected energy and applicator[16], a configuration that is quite different compared to other linacs. The accuracy of the virtual source position for the calculation data can be used to validate accuracy of the Monte Carlo modelling[25]. The reported data show a good agreement between the measured and the RayStation data validating the individual jaw and scraper positions of each applicator/energy of the RayStation model. The observed data show a trend of a minor underestimation of the distance of the virtual source position to the applicator surface in the RayStation model for the smallest applicator pointing out the necessity for the validation of small inserts at extended SSD before clinical implementation.

In general, deviations between RayStation data and measured data remain within NCS15 tolerances implying that RayStation can be used for these non-standard SSD applications without prior dose investigation.

4.2 Dose output for different cutouts

Unshielded electron diodes were selected for the measurement of output factors of the electron fields. Although many articles can be found confirming their over-response to scattered photons compared to conventional dosimeters due to the photoelectric effect in silicon (Z=14)[26,27] analogue articles for incident electron beams are less obvious. Therefore, cross-calibration data were measured using the PTW Roos chamber for the standard cut-outs for all beam energies. The cross-calibration affirmed agreements within individual measurement errors of 2% but an increased response of the electron diode for the 14x14 cm² and 20x20 cm² was observed for all beam energies. Correcting the diode data with the cross-calibrated values for each beam energy and each individual applicator (with the standard cut-out) resulted in an average dose difference reduction between RayStation and the corrected measured data form 1.5%±1.0% to 0.5%±0.8%. Cross-calibration as a method for correcting differences in height setup after every change of applicator is justified as systematic errors are observed in literature when no cross-calibration is performed[18].

The importance of inclusion of the 4 MeV energy in this lies in the fact that 4 MeV is characterized by a different behavior in the relative output factors of different applicators and inserts compared to the other available energies. While the four other energies reach a maximum in dose output for the 10x10cm² applicator, the 4 MeV electron beam is more dose efficient (in cGy/MU) for 14x14cm² and 20x20cm² applicators and much less efficient for a 6x6cm² applicator. All those trends are modelled perfectly.

A significant reduction in efficiency of the 2.5x10cm² by the cutout for the 10x10cm applicator was recorded for all beam energies together with a minor reduction in efficiency for the 4x4cm² and 4x12cm² inserts in the 6x6cm² and 14x14cm² applicators. All these observed trends are very well

modelled by the RayStation model far within NCS tolerances. The average agreement for the inserts on the Elekta applicators is equivalent with data for the Varian Truebeam for the corresponding energies (6-12 MeV)[18]. This study is unique in the reporting of very good agreement for 4 MeV beams.

For the smallest inserts however, PDD measurements have to be performed before clinical release in order to validate their agreement with the Monte Carlo calculations.

4.3 Oblique Incidence

Oblique incidence of the incoming electron beam lowers the distance where the R50 is located, when compared to the "standard R50 value". The R50 value is an indicator for penetration strength of that beam and characterizes the energy of the beam. On perpendicular beam incidence a difference of 1 mm upon the expected R50 value results in a dose difference of 5%. NCS15 report states that within a quality assurance program, the limit on R50 value for perpendicular incidence is 2 mm. Within the QA program at Ghent University Hospital, a tolerance level of only 1 mm upon the "standard R50" value is used, together with an action level when a difference of 2 mm is seen. Analysis of the beam quality in this investigation confirmed the accuracy of the R50 values (on perpendicular incidence) and thus the beam energies. The penetration depth is the most important clinical parameter for the MD while selecting the appropriate energy.

Regarding oblique incidence of the electron beams as investigated in this work, the differences between measured and calculated R50 values are within 1mm much better than the tolerance of 3 mm (NCS15). Also, the shape and absolute values of the calculated curves are in excellent agreement with the measured data. The 4 cm off axis positioning of the diode at SSD=110 cm implies that the measured and calculated data are varying in their off axis position in Beams Eye View from -3.5 cm at Gantry 0° to + 3.5 cm for Gantry 30° value for the diode at 45mm depth.

Validation using a plane parallel ionization chamber (Roos chamber) was performed, through comparison of measured dose over the chamber volume and the calculated average dose. Dose

inhomogeneity within the chamber volume remained below 5%, both in measurement and calculation justifying the use of average dose values for comparison. During the analysis, care was taken to ensure that the calculation voxels coincided perfectly with the chamber contours (cylinder of 12-mm radius an 2-mm height)[28]. For the air vented chamber, ionization values were converted to dose values using one single conversion coefficient for each energy at measurement depth for perpendicular incidence. The results were also in agreement with the NCS tolerances and minor differences were linked to variation in the R50 value of 10 MeV and 12 MeV for the linac at the day of measurement.

4.4 Dose behind heterogeneous media

Dose volume effects are considered as minor, as the calculated dose voxels 2x2x2mm³ are very close in size to the chamber volumes of the linear array (4x4x0.5mm³) . Validation measurements using plane parallel ionization chambers using a Roos chamber for the lung and air inserts and a Markus chamber for the bone inserts were executed, Although the conclusions were similar these results are not reported in detail. Data obtained by linear array measurements are considered more appropriate, because dose inhomogeneity perpendicular to plane parallel chamber axis was more than 10% and therefore far less reproducible. For the data obtained using the linear array, the perturbation of the dose by the linear array is taken into account, while it was included during the scanning of the phantom. Depth dose profiles are influenced by the presence of the linear array as this device is constructed form material with a high Z value. This results in extra dose in front of the array due to backscatter from the linear array. The presence of the measuring device on the CT scan should be assessed prior to measurement, as large devices with high Z values affect the reconstruction of the CT images .

4.4.a Lung

According to the criteria of NCS15 two different regions (δ_2 and δ_4) of the percent depth dose profiles were evaluated. In the photon tail region (δ_4) the dose agreement should be 4%, in the high dose

gradient region (δ_2) and the distance to agreement should be better than 3 mm/10%. All curves for the air phantom and the lung phantoms were within the acceptance criteria of NCS15..

For the high energies δ_2 criteria are applied centrally (10-12 MeV in figure 7 and 6-8-10-12 MeV in figure 8). There the calculation voxels at the level of the linear array are often the best fit or one voxel more distal but no systematic trend for each individual energy is observed indicating the exact positioning of the voxels on each scan and the voxel size are also influencing the results.

These results are identical for all three applicators and for both phantoms, illustrating no field size dependence and no energy dependence of the accuracy of the dose prediction in RayStation. The recorded data also allow for the large applicators (10x10cm² and 14x14cm²) off axis validation at 7.1/8.1 cm depth while the recommended effective density of polystyrene for electron beams equals 0.99[29].

4.4.b Air

In Monte Carlo dose calculations of clinical cases over dosage within and behind air cavities are often observed influencing dose homogeneity on tumor volume behind those cavities[1,5,7,21]. This specific situation is validated by the 12 MeV beams for 10x10 cm² and 14x14 cm² field sizes at SSD = 100 cm. A maximum dose of 1.15 cGy/MU is obtained at the distal boundary of the air cavity.

The linear detector array measurement was situated 1 cm behind the distal boundary of the air cavity. Its presence resulted in an increase in the backscatter in front of the linear array and in an increase of dose at the level of the linear array. This difference of approximately 10% and is not only observed at the level of the planning system, measurements have confirmed it (Roos data versus linear array data). At this depth, the depth dose curve calculated by RayStation results in a fast decreasing value (>5cGy/mm) but still exceeds 1 cGy/MU (1.063 cGy/MU). This high efficiency was confirmed by the measurement of the linear array (1.025 cGy/MU; Figure 6) a value that remains within both NCS tolerances (distance to agreement of 3mm and dose agreement of 10%), confirming the high dose levels behind air cavities.

This excellent agreement is obtained for all three applicators and for the larger 10x10cm² and 14x14cm² applicators a validation of the off-axis data at 6.1 cm depth is obtained.

4.4.c Bone

A high accuracy of the electron dose engine for dose prediction behind high-density materials was shown in the resul

ts. Accordance between measured and calculated profiles right underneath the bone rods and next to them, shows the capability of RayStation to predict dose in heterogeneous media. Since the dose profiles are measured and calculated only 3 mm below the inserts, the excellent agreement validates the Monte Carlo model close to high density interfaces. The three different scans of the phantom with three different inserts with the linear array in its polystyrene slab holder enabled us to validate the data independent of an individual voxel position versus the exact position of the linear array. Indeed while for one phantom the matching voxel resulted for a certain energy in the best agreement, for the second phantom the more distal or proximal gave the best match. Since the distance to agreement tolerance in NCS15 is 3 mm a clinical 2x2x2mm² voxel setting is acceptable both in spatial resolution and calculation time.

While this phantom is only 3.5 cm of polystyrene and due to the cylindrical shape of the rod, off axis validation of the dose prediction for a 14x14cm² field is obtained at a depth of 3.6 cm for 4 data points in GT (inplane) direction of the Linac and 10 data points in AB (crossplane) direction.

5 Conclusions

According to NCS15 for non-standard treatment setups, a dose agreement of 3 % in the δ_1 region, a distance to agreement of 3 mm/10% in the δ_2 region and a dose agreement of 4 % in de δ_4 region has to be obtained between measurements and calculations. This is investigated using different air filled and liquid filled ionization chambers and diodes in several setups for an Elekta Linac providing maximal electron beam energy of 12 MeV and extending as low as 4 MeV. 4 MeV is known for its

challenging behavior both in SSD dependence and dose output versus field size. Since in RayStation's electron beam model, the geometry of the upper part of the treatment head is accounted for by a set of parameters which are common to all linacs models, it is highly relevant to perform detailed validations for this Elekta linac. This validation by ionization chambers and diodes is complementary with the in-vivo verification of individual treatments at the Ghent University Hospital using EBT-films. The results of the validation confirm the accuracy of the electron beam model and Monte Carlo in RayStation for prediction of dose distribution within acceptable timeframes for clinical electron beam treatment planning.

Acknowledgements

The authors wish to thank the bachelor students Silke Vandeputte, Paulien De Bolle, Lina Napoletano and Vicky Desmadryl of the Odisee Hogeschool-Univeristy Brussels for their fine collaboration during the validation process of the Monte Carlo electron modelling in RayStation.

Conflicts of Interest

Erik Traneus is an employee of Raysearch Laboraties AB

Authors Contributions

All authors have made substantial contributions either to the conception and design of the study or to the evaluation of the results and all have been involved either in drafting the manuscript or in revising it critically.

Author to whom correspondence should be addressed. Electronic mail: geert.pittomvils@uzgent.be

References

1. Berbi BJ, *Technical Basis of Radiation Therapy : Practical Clinical Applications*, chapter 7: Clinicial Applications of High-Energy Electrons. Berlin: Springer Verlag; 2006. 157-196
2. Hogstrom KR and Almond PR. Review of electron beam therapy physics. *Phys. Med. Biol.* 2006; 51 (13): R455-R489

3. Zhang A, Wem N, Nurushev T, Burmeister J, Chetty IJ. Comprehensive evaluation and clinical implementation of commercially available Monte Carlo dose Algorithm. *J. Appl. Clin. Med. Phys.* 2013; 14(2), 127-145.
4. Saw CB, Ayyangar KM, Pawlicki T, Korb LJ. Dose distribution consideration of medium energy electron beams at extended source-to-surface distance. *Int. J. Rad. Oncol. Biol. Phys.* 1995; 32(1): 159-164.
5. Ding GX, Cygler JE, Yu CW, Kalach NI, Daskalov G. A comparison of electron beam dose calculation accuracy between treatment planning systems using either pencil beam of a Monte carlo algorithm. *Int. Rad. Oncol. Biol. Phys*. 2005; 63(2), 622-633.
6. Lawrence SL, van Lieshout NHM, Charland PM. Assessment of Eclipse electron Monte Carlo output prediction for various topologies. *J. Appl. Clin. Med. Phys.* 2015; 16(3), 99-106. doi.org/10.1120/jacmp.v16i3.4636
7. Chamberland E, Beaulieu L., Lachance B. Evaluation of an electron Monte Carlo dose calculation alogorithm for treatment planning. *J. Appl. Clin. Med. Phys.* 2015; 16(3), 60-79.
8. Archilbald-Heeren B, Liu G. RayStation Monte Carlo application: evaluation of electron calculations with entry obliquity. *Austr. Phys. Eng. Sci. Med.* 2016; 39, 441-452.
9. Huang JY, Dunkerley D, Smilowitz JB. Evaluation of a commercial Monte Carlo calculation algorithm for electron treatment planning. *J.Appl.Clin.Med.Phys.* 2019, 20(6), 184-193.
10. Kawrakow I, VMC++ Electron and Photon Monte Carlo calculations optimized for Radiation Treatment Planning. in *Advanced Monte Carlo for Radiation Physics, Particle Transport Simulation and Applications.* Edited by Kling A, Barao F, Nakagawa F, Tavora M, Vaz P. Springer Verlag, Berlin Heidelberg 2001. 229-236. https://doi.org/10.1007/978-3-642-18211-2_38
11. Bruinvis IAD, Keus RB, Lenglet WJM et al. *Quality assurance of 3-D treatment planning systems for external photon and electron beams. NCS Report 15*, Nederlandse Commissie voor Stralingsdosimetrie. 2006 (https://doi.org/10.25030/ncs-015)
12. Goudsmit S, J.L. Saunderson JL, Multiple Scattering of Electrons," *Phys. Rev.*, 1940; 57, 24-29.
13. Kawrakow I, Accurate condensed history Monte Carlo simulation of electron transport. I. EGSnrc, the new EGS4 version. *Med.Phys.* 2000; 27(3), 485-498.
14. Bortfeld T, Schlegel W, Rhein B. Decomposition of pencil beam kernels for fast dose calculation in three-dimensional treatment planning. *Med.Phys.* 1993; 20(2), 311-318.
15. Sorcini BB, Hyödynmaa S, Brahme A. The role of phantom and treatment head generated bremsstrahlung in high-energy electron beam dosimetry. *Phys. Med. Biol.* 1996; 31, 2657-2677.
16. van Battum LJ, van der Zee W, Huizinga H. Scattered radiation from applicators in clinical electron beams. *Phys.Med.Biol.* 2003; 48, 2493-2507.
17. DIN 6800-2: Procedures of dosimetry with probe type detectors for photon and electron radiation – Part 2: Ionization chamber dosimetry of high energy photon and electron radiation, DIN (Deutsches Institut fur Normung), 2008.
18. Richmond N., Allen V, Wyatt J, Codling R. Evaluation of the RayStation electron Monte Carlo dose calculation. *Med.Dos.* 2020; 45, 159-167.
19. Aalbers AHL, Hoornaert M-T, Minken A. et al. *Code op Practice of absorbed dose determination in high energy photon and electron beams. NCS Report 18*, Nederlandse Commissie voor Stralingsdosimetrie. 2012 (https://doi.org/10.25030/ncs-018)
20. Martens C, De Wagter C, De Neve W. The value of the LA48 linear ion chamber array for characterization of intensity-modulated beams. *Phys.Med.Biol.* 2001; 46, 1131-1148.
21. Khan FM, Doppke KP, Hogstrom KR, et al. Clinical electron beam dosimetry: Report of AAPM Radiation Therapy Committee Task Group No.25. *Med. Phys.* 1991; 18(1), 73-109.
22. Cygler J, Li XA, Ding GX, Lawrence E. Practical approach to electron beam dosimetry at extended SSD. *Phys. Med. Biol.* 1997; 42, 1505-1514.

538 23. Gibbons JP, Antolak JA, Huq MS et al. Monitor unit calculations for external photon and electron
539 beams: Report of the AAPM Therapy Physics Committee Task Group No. 71. *Med.Phys.* 2014;
540 41(3), 031501.
541 24. O'Shea TP, Foley MJ, Rajasekar D et al. Electron beam therapy at extended source-to-surface
542 distance : a Monte Carlo investigation. *J.Appl.Clin.Med.Phys.* 2008; 9(4), 57-67.
543 25. Douk HS, Aghamiri MR, Ghorbani M et al. Accuracy evaluation of distance inverse square law in
544 determining virtual electron source location in Siemens Primus linac. Rep. Pract. Oncol.
545 Radiother. 2018; 23, 105-113.
546 26. Griesbach I, Lapp M, Bohsung J, Gademan G., Harder D. Dosimetric Characteristics of a new
547 unshielded silicon diode and its application in clinical photon and electron beams. *Med. Phys.*
548 2005; 32, 3750-3754. doi:10.1118/1.2124547
549 27. Francescon P, Beddar S, Satarino N, Das IJ. Calculation of $kf_{clin}Q_{clin}f_{msr}Q_{msr}$ for several small
550 detectors and for two linear accelerators using Monte Carlo simulations. Med. Phys. 2011; 38,
551 6513-6527. doi: 10.1118/1.3660770.
552 28. Butler DJ, Stevenson AW, Wright TE et al. High spatial resolution dosimetric response maps for
553 radiotherapy ionization chambers measured using kilovoltage synchrotron radiation.
554 Phys.Med.Biol. 2015; 60, 8625-8641.
555 29. Gerbi BJ, Antolak JA, Deibel FC et al. Recommendations for clinical electron beam dosimetry:
556 Supplement to the recommendations of Task Group 25. *Med.Phys*. 2009; 36(7), 3229-3279.